Numerical Simulation of Orthogonal Machining of Gallium Nitride via Smoothed Particle Hydrodynamics

Muhammad Haseeb [a], Hasan Aftab Saeed[a] and Imran Sajid S. Ghumman [b]*

[a] College of Electrical & Mechanical Engineering,
National University of Sciences and Technology Islamabad, Pakistan.
[b] Faculty of Mechanical Engineering, HITEC University Taxila, Pakistan.

mhaseeb.me18ceme@student.nust.edu.pk, hasan.saeed@ceme.nust.edu.pk
imran.sajid@hitecuni.edu.pk

**Corresponding Author*

Abstract

Gallium Nitride is one of the best candidates for upcoming industrial revolution due to its superior electrical properties over silicon. In the present work, we investigate the chip formation, cutting force and effective stress in diamond machining of gallium nitride by smoothed particle hydrodynamics approach based on Mohr-Coulomb material model. The comparison of the effective stress as reported by molecular dynamics studies and that predicted by the smoothed particle hydrodynamics simulation demonstrates the effectiveness of the smoothed particle hydrodynamics model.

Keywords: Diamond cutting, Gallium Nitride, Smoothed particle hydrodynamics, Mohr-Coulomb

1. Introduction

Gallium Nitride (GaN), third generation of semiconductor materials, is popular in the industrial and educational fields due to its exceptional properties. Such properties include direct energy gap, wide forbidden band, and high temperature and pressure resistivity. Due to these benefits, devices consisting of GaN components have been mostly used in high power and frequency electronic devices, high electron mobility transistors (HEMT), and ultraviolet/blue/green light emitting diodes [1]. GaN is usually processed by cutting, grinding or mechanical polishing. The hard and brittle material of GaN [2] makes it difficult to machine with conventional machining processes.
Molecular Dynamics has been widely used over the past decade or so to analyze the concerned machining properties and parameters of GaN [3,4,5].
Gu et al. [6] machined materials like GaN, sapphire and micro light emitting diodes by using Ultra-Violet (UV) copper vapor laser which was pulsed at a fixed frequency. They reported that the pulsed UV vapor copper laser can easily be used for micromachining or dicing of such materials. Kim et al. [7] studied the ablation of GaN by ultrashort pulsed laser, and successfully demonstrated the controlled ablation. Nakahama et al. [8] used plasma chemical vaporization machining (CVM) to observe the etching characteristics of GaN and reached the conclusion that less subsurface damage is caused by plasma CVM than RIE (reactive ion etching). Zhang et al. [9] conducted molecular dynamics simulation to investigate the mechanism of subsurface damage during nano grinding process of GaN and provided an insight into low-damage processing of GaN by the subsurface damage mechanism. Huang et al. [10] attempted to nano grind GaN using one-dimensional sinusoidal assisted vibration by molecular dynamics. They found out that high

removal rate and surface finish was achieved for the vibration assisted nano-grinding. Wang et al. [11] simulated abrasive machining for wurtzite GaN and explored the effect of abrasive size change on it. They reached the conclusion that increasing the size of the abrasive increases the plastic deformation which eventually increases atomic temperature, stress and strain. Babi\acute{c} et al. [12] discussed the drilling and dicing issues related to GaN-on-diamond wafers using laser micromachining for radio frequency power transistor applications. Gu et al. [13] reported the use of pulsed UV lasers for the manufacturing of microstructures for GaN in free standing state. They succeeded to create good quality trenches for free-standing GaN. Nowak et al. [14] applied contact loading of the surface and captured the response of homoepitaxially created GaN when it deformed on a nano scale. Guo et al. [15] studied Gallium and Nitride faced GaN in terms of their nanotribological properties using diamond indenter through nano-scratch experiments and suggested that the elastic modulus of N faced GaN was slightly lower than that of Ga faced GaN. Zou et al. [16] executed research on the impact of mechanical action and chemical function, during the chemical-mechanical polishing (CMP) process on the pits that appear on the GaN surface after polishing. They focused on the association between surface characterisation after CMP of GaN substrates and the concentration of the silica (SiO2) abrasive employed for CMP. Qian [17] observed the deformation in wurtzite GaN through molecular dynamics simulations. Slips on the planes were calculated by the investigation of generalized stacking fault energy. Xiang et al. [18] formulated research with the help of molecular dynamics on B4 ceramic to examine the creation of prismatic loops on it due to nanoindentation. Wang et al. [19], after carrying out a study on the mechanical response of the GaN nanowires in their inelastic range, reported that the failure mechanisms are dependent on size and the shuffle set pyramidal planes. Aida et al. [20] revealed the relation between depth of the subsurface damage (SSD) and the diamond abrasive size which was used for GaN substrates for mechanical polishing. They confirmed that the SSD depth decreases as the size of the diamond abrasive is reduced.

Considerable work on GaN has been done in the past using the molecular dynamics approach. In the present research, we establish a 3D smoothed particle hydrodynamics (SPH) model for diamond cutting of GaN based on the Mohr-Coulomb material model which can capture plastic flow and brittle failure. We also find out the cutting forces generated during the machining process.

2. Methodology

2.1 Smoothed Particle Hydrodynamics

Physical problems like fluid flow and transport phenomena are mostly modelled in the Eulerian framework. This modelling approach, utilized in numerical techniques such as the finite difference method, finite volume method and finite element method, requires the use of grids or meshes to solve integral formulations or partial differential equations. Controlling consistency is one of the problems while using approaches that use meshes. This difficulty can especially arise when dealing with complex geometries, mobile interfaces, free surfaces, and topological changes. Remeshing can be done to address these problems, but it is expensive and time-consuming.

In Lagrangian modelling, the system can be subdivided into particles that are finite and in their original intent, they do not share any information with each other. Coordinates of centre of mass define the position and their physical properties as well. These meshless approaches are being

widely used for research purposes resulting in accurate and stable solutions for partial differential equations or integral equations. In the previous decade, there has been a sudden increase in the use of meshless methods for complex problems. Least squares (MLS), Smooth particle hydrodynamics (SPH), and Galerkin method are some of the extensively used meshless numerical methods [21].

In the late 1970s, astrophysics phenomena were studied by Lucy et al. [22] and Ringold et al. [23] by using SPH method for the first time. Later, due to its ability to accommodate the complex attributes of physical problems, it was applied to solid and fluid mechanics problems as well [21]. The basic underlying rule is to subdivide the system into particles. Weighted interpolations are used to give properties to these particles which are in the neighbourhood defined by the domain of influence. The response of the physical quantities in the fixed particle is dependent on the neighbouring particles which are at a radial distance from it as shown in Fig.1.

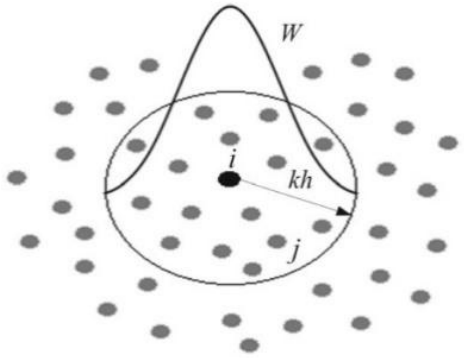

Figure 1: Graphical representation of the kernel and its dominance domain. Physical properties of the reference particle 'i' is affected by the side particle 'j' which lies inside the influenced area [21]

The general mathematical expression for the SPH method is as follows:

$$f_i = \sum_{j=1}^{n} m_j \frac{f_j}{\rho_j} W(X_i - X_j, h) \#(1)$$

Where:

f_i Fixed particle's approximated value

f_j Neighbouring particle's approximated value

m_j Neighbouring particle's mass

ρ_j Neighbouring particle's density

X_i Fixed particle's location

X_j Neighbouring particle's location

$W(X_i - X_j, h)$ Value of kernel found at the respective location

n Total number of particles acting as neighbours

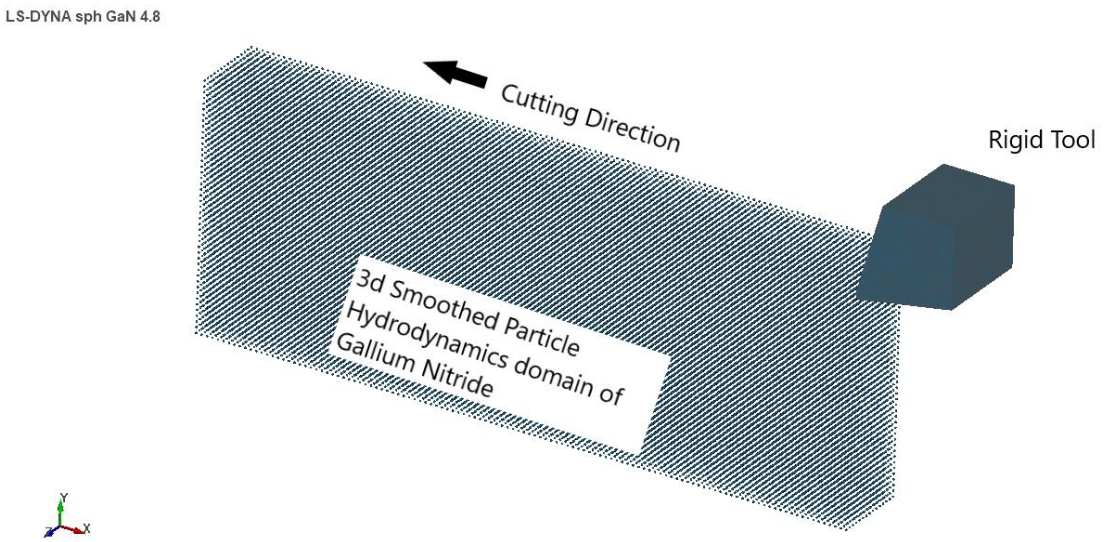

Figure 2: Basic set-up of Numerical Simulation in ANSYS/LS-DYNA

Fig. 2 shows a 3D model of orthogonal machining of GaN, which consists of a GaN workpiece and a diamond cutting tool in ANSYS/LS-DYNA. The specimen has dimensions of 0.008 m length, 0.003 m height and 0.001 m thickness. In the application of the SPH scheme, the specimen's bottom is fully restricted in order to avoid any rigid body motion in the cutting process. The diamond cutting tool, being treated as rigid body, has a relief angle of 0.1745 rad, nose radius of the tool is 0.0001 m and the rake angle is 0.2618 rad.

Prior to the cutting process, the tool tip is kept at an offset of 0.0001 m from the top right corner of the specimen with a 0.0002 m depth of cut. The tool movement is controlled by providing a load curve and it is expected that the specimen will go from elastic deformation to plastic deformation, which will be followed by brittle failure.

2.2 Mohr-Coulomb material model

The Mohr-Coulomb material model is extensively used in geomechanics. Rock, soil, and aggregate materials are modeled by this method to show their mechanical behavior in their natural or artificial ambience. Masonry structures made of concrete and similar materials, which fail due to stress concentrations or because of weak regions, can be effectively modeled by this material model. Examples of such structures include footings, pilings, and seismic systems.

Plastic deformation after an initial elastic stage is displayed by materials that follow the Mohr-Coulomb material model. Unloading from the plastic deformation results in the recovery of elastic stage. Phenomena such as shear loading and volumetric plasticity, realized when the particles move past one another in a domain can be traced back to the material behavior at the microscopic level. Plastic deformations start when the internal friction among particles is dominated by the shear force applied. Being a wurtzite crystal, GaN suits the applicability of this method. Normal force between the particles defines the frictional resistance of such materials which can be modeled by Mohr-Coulomb material model [24]. Material data for GaN were taken from GRANTA/ANSYS Library [25].

Mathematically, Mohr-Coulomb material model is represented by the following equations:

$$| \tau | = S_\circ + \sigma \tan\phi \quad (2)$$

$$(\sigma_1 - \sigma_3) = (\sigma_1 + \sigma_3) \sin\phi + 2S_\circ \cos\phi \quad (3)$$

$$\tau_m = f(\sigma_m) \quad (4)$$

Where:

τ	Shear stress
$S_\circ$	Inherent shear strength of material also called cohesion value
σ	Normal stress
ϕ	Internal friction angle
σ_1	Major principal stress
σ_3	Minor principal stress
τ_m	Mean shear stress
σ_m	Mean principal stress
α_f	Angle between minor principal stress plane and failure plane

When represented in Mohr diagram, Eq. 2 is a straight line at a friction angle ϕ from the normal stress plane σ as shown in Fig. 3. Eq. 3 is an alternative form of Eq. 2 which can be obtained by making the Mohr circle tangent to the line which has a stress state linked with failure. Eq. 4 shows that on the $\tau - \sigma$ plane, the Mohr envelope can be constructed and the tangency of the circle having diameter $(\sigma_1 - \sigma_3)$ to the failure envelope $\tau = g(\sigma)$ will result in failure.

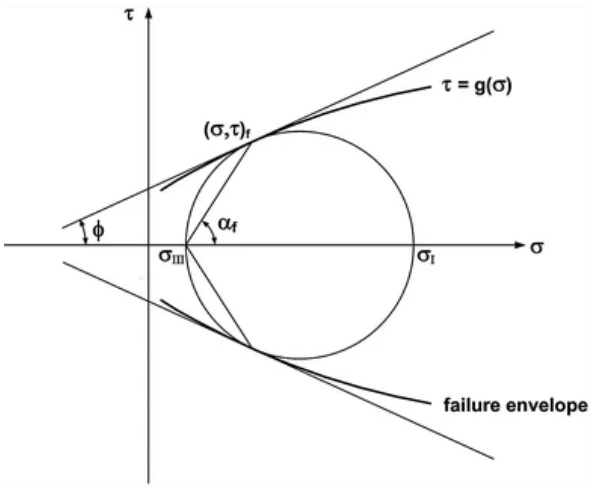

Figure 3: Mohr Diagram and failure envelops [26]

3. Results and discussion

SPH simulation of orthogonal cutting was carried out to investigate the effective stresses, chip formation and cutting forces during conventional diamond tool cutting. Figs. 4a to 4f represent the snapshots of the process at different time intervals, showing the stress contours at various stages of the process. At the initial stages of the cutting process, there is no chip formation (Fig. 4c), yet the material undergoes pure plastic deformation. High concentration of stress can be seen

near the vicinity of tool tip. Upon further movement of tool along the cutting direction, there is a saw-tooth chip formed also called ductile mode cutting which immediately undergoes brittle material removal as shown in Fig. 4d.

The local Von Mises stress distribution in the specimen changes with the progressive movement of the diamond tool. Stresses higher than 6×1010 Pa are generated, which are concentrated ahead and underneath the cutting tip. Von Mises stress decreases after the passage of the tool in the machined area, leaving residual stresses behind.

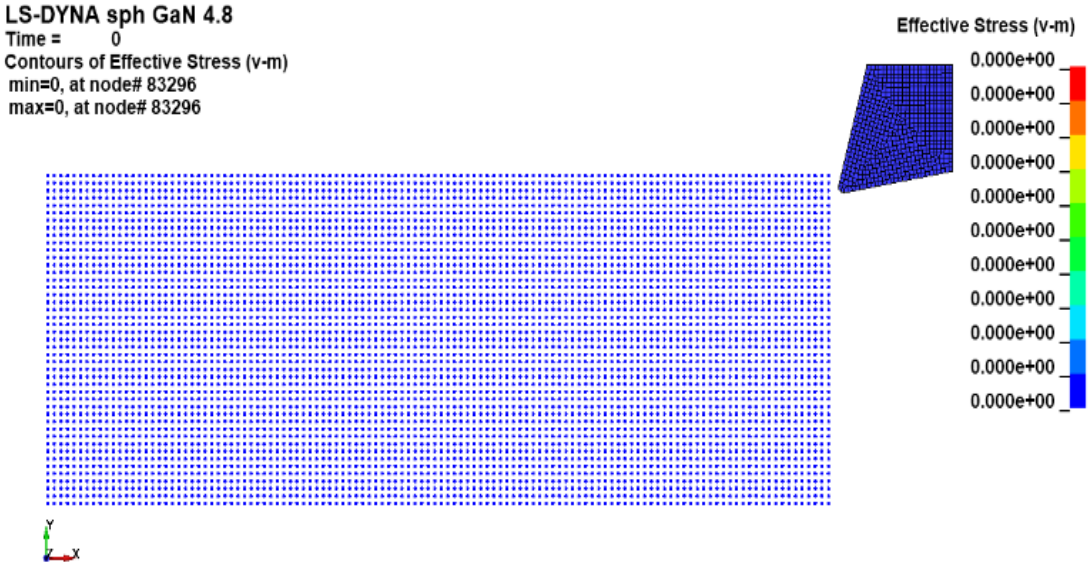

Figure 4a: Maximum Stress = 0 Pa at time = 0 s

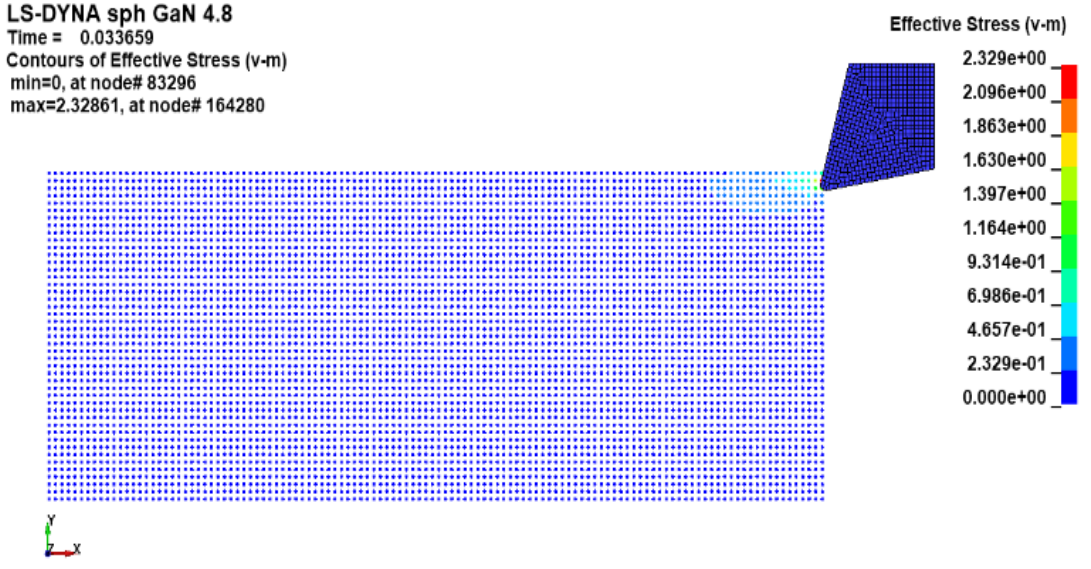

Figure 4b: Maximum Stress = 2.329×10^{9} Pa at time = 3.3659×10^{-5} s

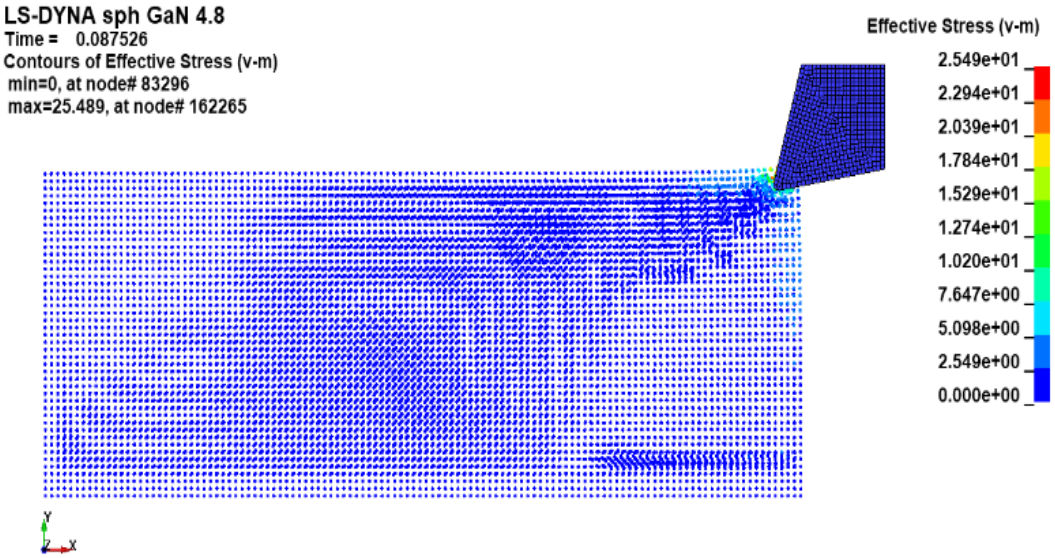

Figure 4c: Maximum Stress = 2.549×10^{10} Pa at time = 8.7526×10^{-5} s

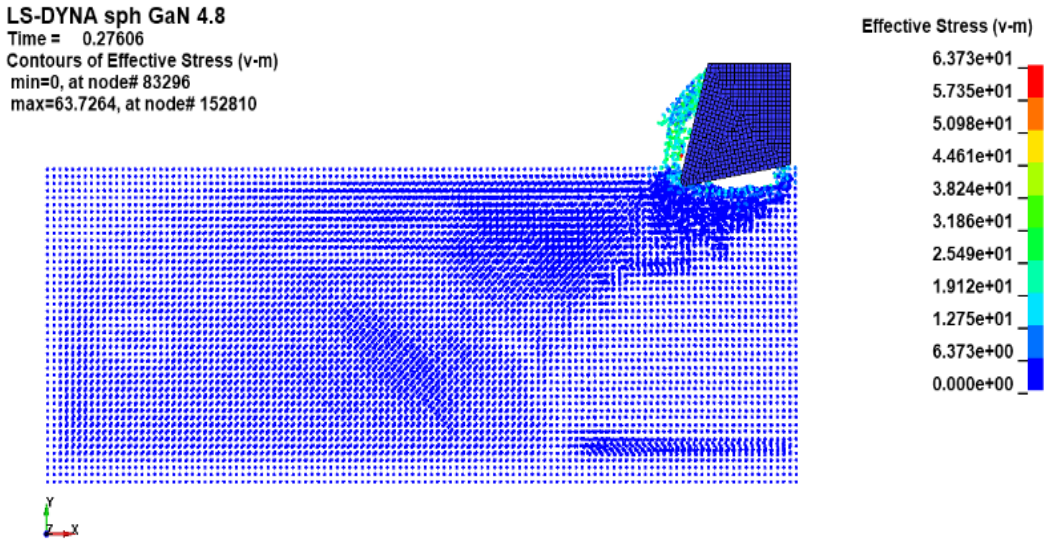

Figure 4d: Maximum Stress = 6.373×10^{10} Pa at time = 2.7606×10^{-4} s

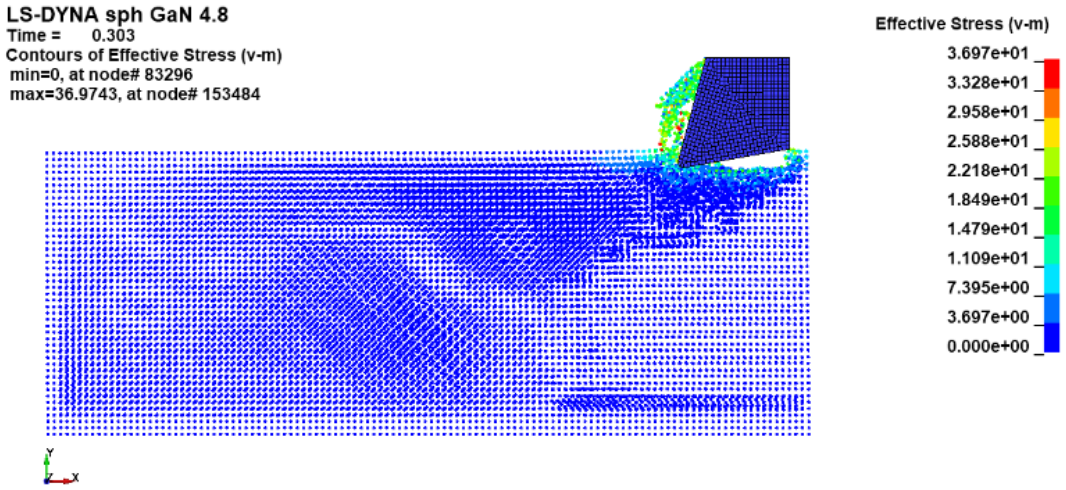

Figure 4e: Maximum Stress = 3.697×10^{10} Pa at time = 3.03×10^{-4} s

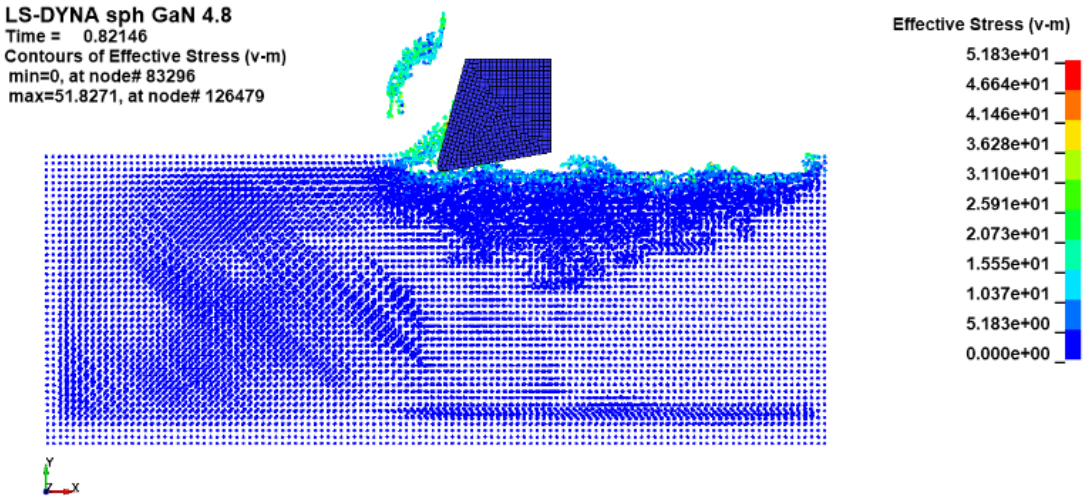

Figure 4f: Maximum Stress = 5.183×10^{10} Pa at time = 8.2146×10^{-4} s

Fig. 5 shows the scattered graph showing the stress distribution inside the SPH domain of GaN as numerical simulation progresses. The small horizontal portion at the start of the simulation shows that the contact between diamond tool and the GaN workpiece has not been established yet. Once the tool comes in contact with the workpiece, the stresses pile up till point A. Once the Von Mises stress reaches point A, a sudden erosion of a bunch of SPH particles occur which can be classified as a dominant brittle failure which matches with the [3]. In the process, the stress decreases from 6.373×10^{10} Pa to 3.82×10^{10} Pa. For the next interval, due to the continuous forward movement of tool, equivalent stresses are again accumulated till point B and brittle failure occurs again resulting in lowering of the Von Mises stress. These cycles repeat till the end time of the simulation is reached. As the SPH approach is a particle-based approach, any particle reaching Mohr-Coulomb failure criteria will be eroded. An average peak value of equivalent Von Mises stress (at points A, B, C, D and E) is found to be 5.955×10^{10} Pa at which brittle failure occurs which matches with the reported value of 6.4×10^{10} Pa [1].

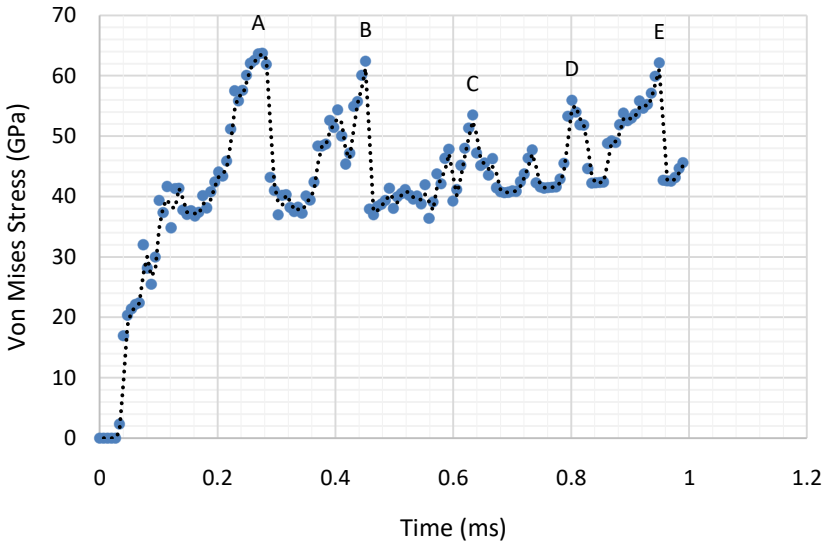

Figure 5: Equivalent Von Mises Stress vs Time

The contact force, as shown below in Fig. 6, with 0.0002 m depth of cut peaks at 2000 N but decreases to 1830 N when averaged over the total interval. However, this cutting force can be easily reduced by using small depth of cuts, slow movement of cutting tool along the cutting axis and decreased nose tip radius of tool.

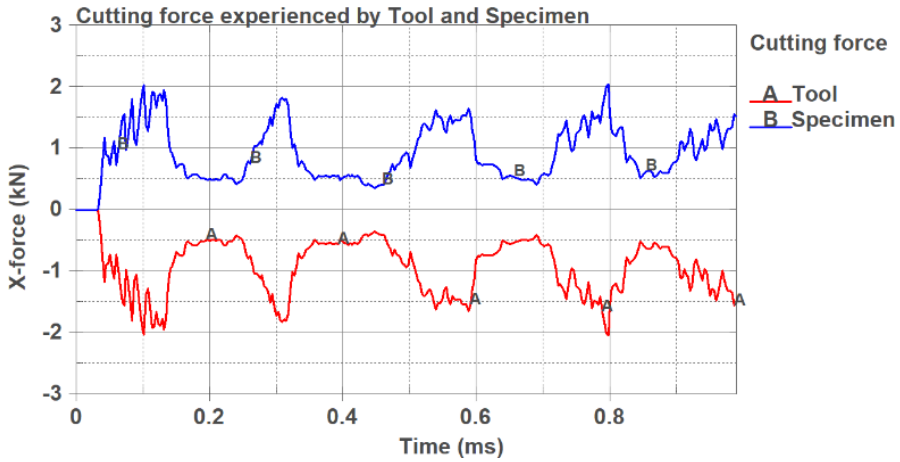

Figure 6: Contact forces generated during simulation

4. Conclusion

This study demonstrates the feasibility of combining smoothed particle hydrodynamics with the Mohr-Coulomb material model to predict the machining behavior of Gallium Nitride as an alternate method to the computationally expensive Molecular Dynamics. As a further result of the framework developed, it is concluded that brittle mode material removal will be the primary cause of material removal during the orthogonal machining of Gallium Nitride**.**

Contribution of Authors

Muhammad Haseeb: Conceptualization, data curation, methodology, original draft, simulation; **Hasan Aftab Saeed**: Methodology, editing of manuscript; **Imran Sajid S. Ghumman**: Data curation, simulation.

References

[1] Y. Wang, S. Tang, and J. Guo, "Molecular dynamics study on deformation behaviour of monocrystalline GaN during nano abrasive machining," Applied Surface Science, vol. 510, p. 145492, Apr. 2020, doi: 10.1016/J.APSUSC.2020.145492.

[2] Q. Jiang, L. Zhang, and C. Yang, "Research on material removal mechanism and radial cracks during scribing single crystal gallium nitride," Ceramics International, vol. 47, no. 11, pp. 15155–15164, Jun. 2021, doi: 10.1016/J.CERAMINT.2021.02.074.

[3] Y. Wang and J. Guo, "Effect of abrasive size on nano abrasive machining for wurtzite GaN single crystal via molecular dynamics study," Materials Science in Semiconductor Processing, vol. 121, Jan. 2021, doi: 10.1016/j.mssp.2020.105439.

[4] Y. Xu, F. Zhu, M. Wang, X. Liu, and S. Liu, "Molecular dynamics simulation of gan nano-grinding," 2018 IEEE 20th Electronics Packaging Technology Conference, EPTC 2018, pp. 468–472, Dec. 2018, doi: 10.1109/EPTC.2018.8654336.

[5] J. Guo, J. Chen, Y. Lin, Z. Liu, and Y. Wang, "Effects of surface texturing on nanotribological properties and subsurface damage of monocrystalline GaN subjected to scratching investigated using molecular dynamics simulation," Applied Surface Science, vol. 539, p. 148277, Feb. 2021, doi: 10.1016/J.APSUSC.2020.148277.

[6] E. Gu et al., "Micromachining and dicing of sapphire, gallium nitride and micro LED devices with UV copper vapour laser," Thin Solid Films, vol. 453–454, pp. 462–466, Apr. 2004, doi: 10.1016/J.TSF.2003.11.133.

[7] T. Kim et al., "Femtosecond laser machining of gallium nitride," Materials Science and Engineering: B, vol. 82, no. 1–3, pp. 262–264, May 2001, doi: 10.1016/S0921-5107(00)00790-X.

[8] Y. Nakahama et al., "Etching characteristics of GaN by plasma chemical vaporization machining," Surface and Interface Analysis, vol. 40, no. 12, pp. 1566–1570, Dec. 2008, doi: 10.1002/SIA.2955.

[9] C. Zhang, Z. Dong, S. Yuan, X. Guo, R. Kang, and D. Guo, "Study on subsurface damage mechanism of gallium nitride in nano-grinding," Materials Science in Semiconductor Processing, vol. 128, p. 105760, Jun. 2021, doi: 10.1016/J.MSSP.2021.105760.

[10] Y. Huang, M. Wang, Y. Xu, and F. Zhu, "Investigation of vibration-assisted nano-grinding of gallium nitride via molecular dynamics," Materials Science in Semiconductor Processing, vol. 121, p. 105372, Jan. 2021, doi: 10.1016/J.MSSP.2020.105372.

[11] Y. Wang and J. Guo, "Effect of abrasive size on nano abrasive machining for wurtzite GaN single crystal via molecular dynamics study," Materials Science in Semiconductor Processing, vol. 121, p. 105439, Jan. 2021, doi: 10.1016/J.MSSP.2020.105439.

[12] D. I. Babić et al., "Laser machining of GaN-on-diamond wafers," Diamond and Related Materials, vol. 20, no. 5–6, pp. 675–681, May 2011, doi: 10.1016/J.DIAMOND.2011.03.017.

[13] E. Gu et al., "Microfabrication in free-standing gallium nitride using UV laser micromachining," Applied Surface Science, vol. 252, no. 13, pp. 4897–4901, Apr. 2006, doi: 10.1016/J.APSUSC.2005.07.117.

[14] R. Nowak, "Nanoindentation study on insight of plasticity related to dislocation density and crystal orientation in GaN," Applied Physics Letters, vol. 101, no. 20, p. 201901, Nov. 2012, doi: 10.1063/1.4767372.

[15] J. Guo, C. Qiu, H. Zhu, and Y. Wang, "Nanotribological Properties of Ga- and N-Faced Bulk Gallium Nitride Surfaces Determined by Nanoscratch Experiments," Materials 2019, Vol. 12, Page 2653, vol. 12, no. 17, p. 2653, Aug. 2019, doi: 10.3390/MA12172653.

[16] Ariz. ICPT 2015 Chandler, American Vacuum Society Northern California Chapter, Center for Advanced Materials Processing, Institute of Electrical and Electronics Engineers, Ariz. International Conference on Planarization/CMP Technology 2015.09.30-10.02 Chandler, and Ariz. ICPT 2015.09.30-10.02 Chandler, "2015 International Conference on Planarization/CMP Technology (ICPT) Sept. 30, 2015-Oct. 2, 2015," 2015.

[17] Y. Qian, F. Shang, Q. Wan, and Y. Yan, "A molecular dynamics study on indentation response of single crystalline wurtzite GaN," Journal of Applied Physics, vol. 124, no. 11, p. 115102, Sep. 2018, doi: 10.1063/1.5041738.

[18] H. Xiang, H. Li, T. Fu, C. Huang, and X. Peng, "Formation of prismatic loops in AlN and GaN under nanoindentation," Acta Materialia, vol. 138, pp. 131–139, Oct. 2017, doi: 10.1016/J.ACTAMAT.2017.06.045.

[19] R. J. Wang, C. Y. Wang, Y. T. Feng, and C. Tang, "Mechanical responses of a-axis GaN nanowires under axial loads," Nanotechnology, vol. 29, no. 9, p. 095707, Jan. 2018, doi: 10.1088/1361-6528/AAA64D.

[20] H. Aida et al., "Evaluation of subsurface damage in GaN substrate induced by mechanical polishing with diamond abrasives," Applied Surface Science, vol. 292, pp. 531–536, Feb. 2014, doi: 10.1016/J.APSUSC.2013.12.005.

[21] C. Alberto. Dutra Fraga Filho, "Smoothed Particle Hydrodynamics: Fundamentals and Basic Applications in Continuum Mechanics.," p. 167, 2018.

[22] L. B. Lucy, Lucy, and L. B., "A numerical approach to the testing of the fission hypothesis.," AJ, vol. 82, pp. 1013–1024, Dec. 1977, doi: 10.1086/112164.

[23] R. A. Gingold and J. J. Monaghan, "Smoothed particle hydrodynamics: theory and application to non-spherical stars," Monthly Notices of the Royal Astronomical Society, vol. 181, no. 3, pp. 375–389, Dec. 1977, doi: 10.1093/MNRAS/181.3.375.

[24] "Sample Libraries." https://ansyshelp.ansys.com/account/secured?returnurl=/Views/Secured/corp/v202/en/wb_eda/eda_ansys_matlib.html?q=geomechanical (accessed Aug. 28, 2021).

[25] "Ansys Granta: Materials Information Management." https://www.ansys.com/products/materials (accessed Aug. 29, 2021).

[26] J. F. Labuz and A. Zang, "Mohr–Coulomb Failure Criterion," Rock Mechanics and Rock Engineering 2012 45:6, vol. 45, no. 6, pp. 975–979, Jul. 2012, doi: 10.1007/S00603-012-0281-7.